PAPER

Passively morphing ornithopter wings constructed using a novel compliant spine: design and testing

Smart Mater. Struct. **21** (2012) 094028 (9pp) doi:10.1088/0964-1726/21/9/094028

Passively morphing ornithopter wings constructed using a novel compliant spine: design and testing

A A Wissa[1], Y Tummala[2], J E Hubbard Jr[1] and M I Frecker[2]

[1] Department of Aerospace Engineering, University of Maryland and The National Institute of Aerospace, Hampton, VA, USA
[2] Department of Mechanical and Nuclear Engineering, The Pennsylvania State University, University Park, PA, USA

E-mail: awissa@umd.edu

Received 31 December 2011, in final form 21 April 2012
Published 31 August 2012
Online at stacks.iop.org/SMS/21/094028

Abstract
Ornithopters or flapping wing uncrewed aerial vehicles (UAVs) have potential applications in civil and military sectors. Amongst the UAVs, ornithopters have a unique ability to fly in low Reynolds number flight regimes and also have the agility and maneuverability of rotary wing aircraft. In nature, birds achieve such performance by exploiting various wing kinematics known as gaits. The objective of this work is to improve the steady level flight performance of an ornithopter by implementing a continuous vortex gait using a novel passive compliant spine inserted in the ornithopter's wings. This paper presents an optimal compliant spine concept for ornithopter applications. A quasi-static design optimization procedure was formulated to design the compliant spine. Finite element analysis was performed on a first generation spine and the spine was fabricated. This prototype was then tested by inserting it into an ornithopter's wing leading edge spar. The effect of inserting the compliant spine into the wings on the electric power required, the aerodynamic loads and the wing kinematics was studied. The ornithopter with the compliant spines inserted in its wings consumed 45% less power and produced an additional 16% of its weight in mean lift compared to the same ornithopter without the compliant spine. The results indicate that this passive morphing approach is promising for improved steady level flight performance.

(Some figures may appear in colour only in the online journal)

Nomenclature

δ	Wing tip to spine tip bending deflection scaling factor
φ	Contact angle of the compliant joint (degrees)
F	Load applied on a compliant spine design (N)
F_{int}	Measured integrated force acting on test ornithopter during mid upstroke (N)
g	Horizontal distance between the contact surfaces (m)
g_c	Contact gap between the contact surfaces (m)
R_{in}	Distance of a control point on the inner surface of a single compliant hinge (m)
R_{out}	Distance of a control point on the outer surface of a single compliant hinge (m)
$b_{\text{ornithopter}}$	Wing span of the test ornithopter (m)
$b_{\text{cockatiel}}$	Wing span of a cockatiel (m)
$Z_{\text{cockatiel}}$	Cockatiel's wing tip bending deflection (m)
$Z_{\text{deflection}}$	Compliant spine tip bending deflection (m)
Z_{req}	Required tip deflection of a compliant spine to imitate CVG (m)

1. Introduction

Over the last few decades, flapping wing uncrewed aerial vehicles (UAVs), or ornithopters, have shown the potential

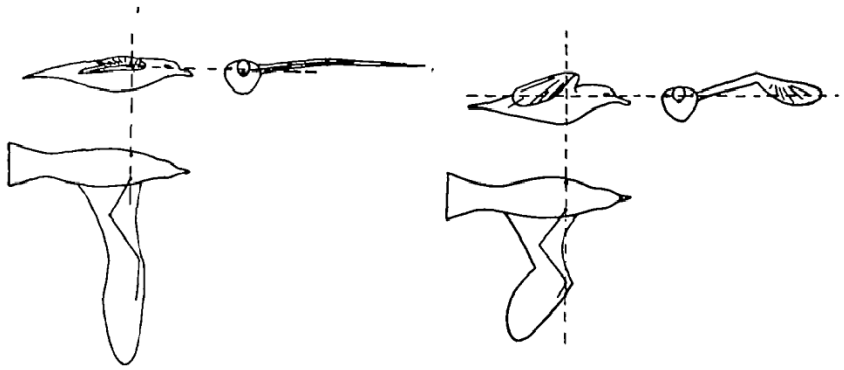

Figure 1. During the continuous vortex gait the wings are fully extended at mid downstroke (left) and bent, twisted and swept at mid upstroke (right) [9].

for advancing and revolutionizing UAV performance in both the civil and military sectors [1]. An ornithopter is unique in that it can combine the agility and maneuverability of rotary wing aircraft with excellent performance in low Reynolds number flight regimes. These traits could yield optimized performance over multiple mission scenarios. Nature achieves such performance in birds using wing gaits that are optimized for a particular flight condition [2, 3].

The goal of this work is to improve the performance of ornithopters during steady level flight using a novel passive morphing approach. The key activities in achieving this goal as presented in this paper are as follows:

- Defining an architecture for passive morphing using compliant mechanisms.
- Developing thorough design optimization algorithms for the compliant mechanism.
- Fabricating and integrating the compliant mechanism into a test ornithopter.
- Comparing the performance of the ornithopter with and without the compliant mechanism to investigate its effect on the steady level flight performance.

Current state of the art designs for wing morphing utilize rigid-link mechanisms or they involve active morphing techniques, such as rigid four-bar mechanisms [4–6]. In contrast to rigid-link mechanisms and active approaches, the focus of the current paper is on the implementation of a novel passive morphing technique using nonlinear compliant mechanisms. When compared to active morphing, passive morphing mechanisms require no additional energy expenditure, and have minimal weight addition and complexity. Moreover, there is no phase lead/lag between the flapping and the morphing mechanisms, as the morphing is only due to the aerodynamic loads experienced by the ornithopter during flight.

The benefits and efficacy of passive wing morphing attained by introducing an asymmetry in the leading edge wing spar kinematics during the up and down strokes has been investigated [7, 8]. Billingsley *et al* installed passive torsional springs in the leading edge spar at the wing half span to exploit the advantages of wing surface area reduction during the upstroke [8]. These springs were designed to deflect on the upstroke only and lock during the downstroke. Wing bending during the upstroke reduces the wing relative area (i.e., the wing area perpendicular to the flapping motion), which in turn mitigates the drag penalties experienced by the test ornithopter during this portion of its wing beat cycle.

While the results of Billingsley's experiment showed a 300% increase in net lift, there were also significant thrust penalties. It was concluded that more sophisticated wing kinematics are required in order to maintain the lift gains while mitigating thrust penalties thus improving the overall aerodynamic performance of the ornithopter. The desired kinematics can be found in natural avian flyers. A bio-inspired gait known as the continuous vortex gait (CVG) is shown in figure 1 [9]. A detailed discussion of the kinematics of the CVG can be found in [2] and [3]. The advantage of using the CVG is that it is an avian gait that can be implemented passively because it requires motion in only one major joint, namely the wrist.

In order to implement the CVG on a test ornithopter and to achieve improved performance, specific wing kinematics are required. The outer section of the wing has to bend, sweep and twist simultaneously during the upstroke, while remaining fully extended during the downstroke. The wrist is the primary joint responsible for the radical shape changes in the CVG gait, thus a compliant spine was placed where an avian wrist would exist, namely at 37% of the wing half span [2]. Figure 2 shows a schematic of the compliant spine and its location along the leading edge spar of an ornithopter.

The compliant spine (CS) is a novel monolithic, nonlinear compliant mechanism. Compliant mechanisms have numerous advantages over rigid-link mechanisms. They are easy to manufacture and cheaper than their rigid-link counterparts because they are usually monolithic in nature. During the upstroke, the compliant spine must have a linear stiffness, which allows the wing to morph in the bending direction; while during the downstroke; it must become very stiff, mimicking a rigid spar. A schematic illustrating the desired stiffness of a compliant spine compared to the rigid spar and to a torsional spring [8] is shown in figure 3(a) for one flapping cycle. Figure 3(b) shows a CS design with three compliant joints (CJs). Note that this design is flexible

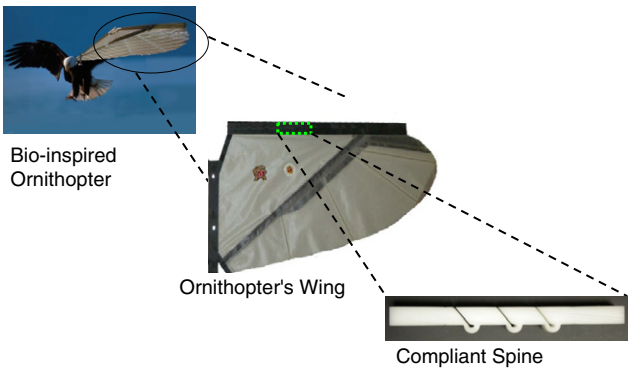

Figure 2. The compliant spine is inserted into the leading edge spar to mimic the function of an avian wrist.

in bending during the upstroke direction because of the compliance of the semi-circular compliant hinges (CHs), and it is very stiff in bending during the downstroke direction because the slanted faces come into contact with one another.

The remainder of this paper is organized as follows: design optimization of compliant spine designs using quasi-static analysis is described in section 2. A proof of concept prototype was evaluated experimentally, and the performance of the ornithopter with and without the compliant spine is compared in section 3.

2. Compliant spine quasi-static analysis

An optimization procedure where the spine was subject to quasi-static loads was implemented in order to design a single compliant hinge with a single compliant joint [10].The parameters that affect the performance of a compliant spine are the number of compliant joints and the shape of each compliant joint. The design parameters that affect the joint's stiffness during the upstroke are related to the shape of the compliant hinge, while the design parameters that affect the downstroke stiffness are related to the geometry of its contact surfaces. A single compliant joint is shown in figure 4 where the inner and outer surfaces of the compliant hinge are assumed to be semi-circles.

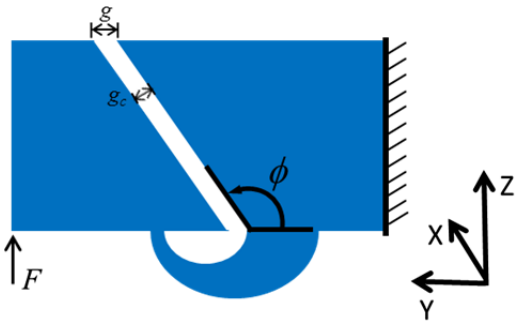

Figure 4. The design parameters that affect the performance of the compliant spine during the upstroke are the shape of the compliant hinge. The parameters affecting the downstroke are the contact gap size (g_c), and the contact angle (φ). Loading and boundary conditions for downstroke analysis are also shown.

2.1. Downstroke quasi-static analysis

The geometry of the contact surfaces is defined by the contact angle (φ) and contact gap (g_c), which is the perpendicular distance between the slanted surfaces shown in figure 4. The parameter g, is the horizontal distance between the slanted surfaces and is related to the contact gap as presented in equation (1).

$$g_c = g * \sin\ (180^\circ - \varphi). \tag{1}$$

The effects of the contact gap and contact angle on the downstroke bending deflection ($Z_{\text{deflection}}$) are considered initially. To understand the effect of the contact gap on downstroke stiffness, finite element analysis simulations of a

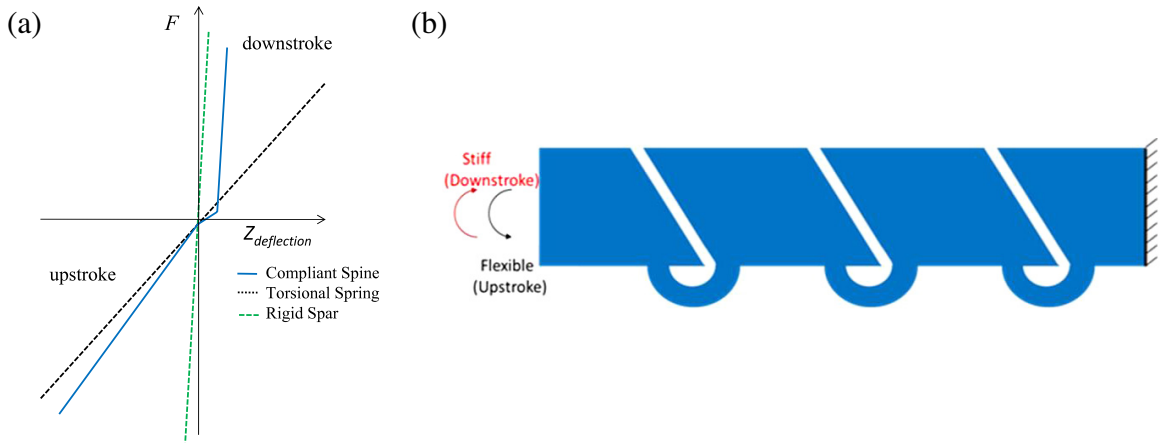

Figure 3. (a) The desired stiffness of the compliant spine is nonlinear. It is stiff in the downstroke direction, similar to a rigid spar, and flexible in the upstroke direction, similar to a torsional spring. Here the Y-axis represents the forces (F) during a flapping cycle and the X-axis ($Z_{\text{deflection}}$) represents the compliant spine tip bending deflection. (b) A compliant spine with three compliant joints is flexible in bending in the upstroke direction due to the presence of the compliant hinges, and stiff during the downstroke due to the meshing of the contact surfaces during flapping.

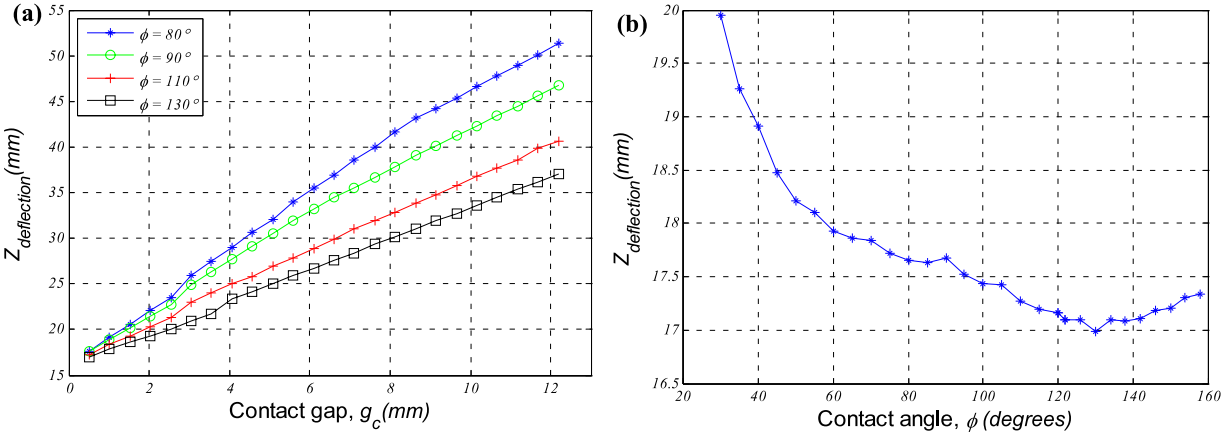

Figure 5. (a) Effect of the contact gap (g_c) and (b) the contact angle (φ) at a gap size of 0.5 mm on the tip bending deflection ($Z_{deflection}$) of a single compliant joint during downstroke. The figures show that the smallest possible contact gap and a contact angle of 130° are desired in order to minimize the bending deflection ($Z_{deflection}$) during the downstroke.

single compliant joint were conducted with varying contact gaps of $g_c = 0.5$ mm (0.02″) to 12.2 mm (0.48″) in steps of 0.5 mm (0.02″) while fixing the contact angle. In addition, another simulation was conducted with varying contact angles of 30°–145° in steps of 5° while fixing the contact gap. This process was performed for all of the possible combinations of contact gap and angle of contact elements. The loading and boundary conditions used for this analysis are shown in figure 4, where the force, F, is a static load applied to the compliant joint. Since this is a design study, the magnitude of F was chosen randomly to be 667.23 N (150lbf) based on the dimensions of the CJ used, such that the contact surfaces come into contact even when the contact gap is as large as 12.2 mm (0.48″). The material that was selected for the compliant spine was DuPont Delrin™ 100ST. Delrin was chosen because of its good fatigue properties, elastic strength, manufacturability and availability. Multi-linear isotropic material properties of Delrin were used during the analysis; the yield strength was assumed to be 45 MPa [11, 12]. Large displacement analysis and Plane42 elements were used in ANSYS during the simulation. Conta172 and Targe169 were used as contact and target elements respectively during the contact pair creation. The maximum nodal z-displacement observed after the contact was taken to be the corresponding $Z_{deflection}$ of each of the designs, the z direction is as shown in figure 4.

Figures 5(a) and (b) show the effect of the contact gap (g_c) and the contact angle (φ), respectively, on $Z_{deflection}$ in a single compliant joint during the downstroke. It is evident from figure 5(a) that as g_c increases, $Z_{deflection}$, for a given contact angle, also increases. This means that the contact gap must be as small as possible in order to achieve the least $Z_{deflection}$ during downstroke. Also, from the same figure, it should be noted that as the angle of contact elements (φ) increases, $Z_{deflection}$ decreases. Figure 5(b) shows the $Z_{deflection}$ of a single compliant joint during the downstroke as a function of contact angle (φ) for a contact gap, g_c, of 0.5 mm. As seen in this plot, the $Z_{deflection}$ is at a minimum when the contact angle is 130°.

2.2. *Upstroke quasi-static analysis*

During upstroke, the compliant spine should mimic the function of an avian wrist and thus achieve the desired bending deflection. In order to optimize the compliant spine for the upstroke condition, both the required bending deflection of the compliant spine and the equivalent load acting on the compliant spine must be estimated. The wing tip bending deflections of a cockatiel during a flapping cycle were captured using a camera and digitized [13]. The equivalent desired ornithopter wing tip deflections were attained by scaling the cockatiel's wing tip deflections using the ratio between the ornithopter's and the cockatiel's wing spans, $b_{ornithopter}$ and $b_{cockatiel}$, respectively. Then the bending deflection of the ornithopter's wing tip was scaled to obtain the desired bending deflection at the spine tip using a scaling parameter (δ). At mid upstroke, it is assumed that the wing bends linearly starting from the CS root. In the compliant spine-spar assembly, the flexible member that causes bending of the wings is the compliant spine. The bending deformation in the rigid carbon fiber spar is minimal. Hence, tip deflection of the wing occurs due to the bending of the compliant spine alone. This compliant spine's bending deflection is translated to the wing tip linearly because of the spar that connects the tip of the compliant spine and the wing tip. It is also assumed that the spar connecting the wing root and CS root is horizontal at this position. Based on these assumptions, the scaling parameter (δ) is the ratio of the CS length to the length of the wing from CS root to wing tip and was determined to have a value of 0.189 [10]. Using these scaling parameters, the minimum desired deflection (Z_{req}) of a CS such that the wing achieves a bending deflection that is corresponding to that of a cockatiel performing the CVG was calculated to be 8.42 mm using equation (2). Equation (2) shows the relationship between the cockatiel's wing tip bending deflection, $Z_{cockatiel}$, and the minimum desired CS tip bending deflection at mid upstroke.

$$Z_{req} = \delta * \frac{b_{ornithopter}}{b_{cockatiel}} * Z_{cockatiel}. \quad (2)$$

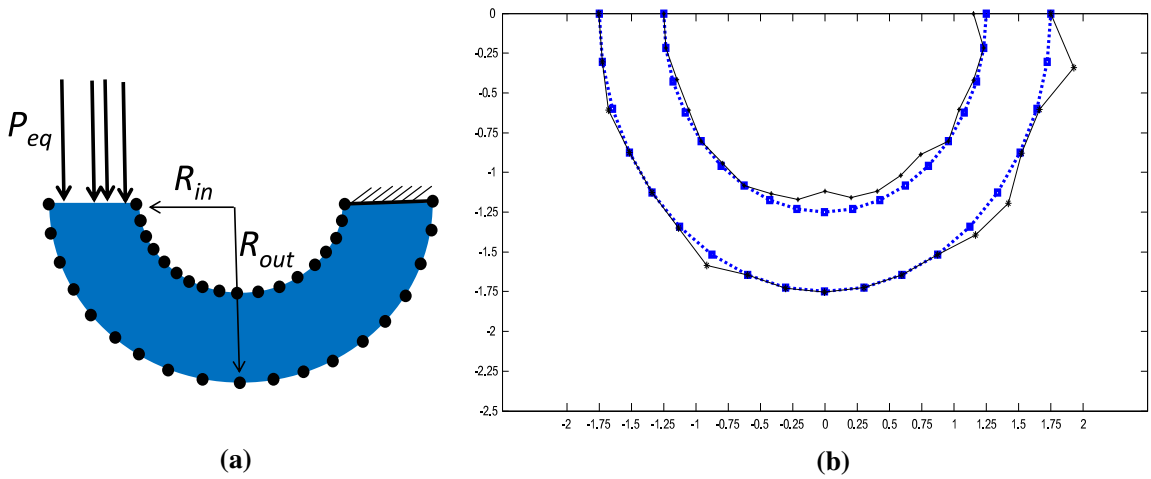

(a) **(b)**

Figure 6. (a) Compliant hinge shape optimization (quasi-static) design parameters and loading conditions. The black dots are the control points that determine the shape of the compliant hinge. (b) Optimal compliant hinge shape (shown as black lines) resulting from the optimization and reference semi-circular hinge (shown as blue dotted lines).

The shape of a single compliant hinge was designed using the quasi-static multi-objective optimization problem described in [10]. The objectives of this optimization problem are to minimize the mass of the hinge, the error in bending deflection as compared to the desired bending deflection, and the error in maximum stress compared to the maximum allowable stress. Nonlinear (approximated as multi-linear) material properties of Delrin, large displacement analysis and Plane42 elements in ANSYS were used for the finite element simulations [11, 12]. The loading and boundary conditions applied to each of the designs are shown in figure 6(a), where P_{eq} is the equivalent pressure applied on the hinge. This pressure is calculated by dividing the static load, F (shown in figure 4), by the area on which the pressure was applied. To estimate the magnitude of F, previous experimental results using an ornithopter without compliant spine were used. The integrated force acting on the test ornithopter at mid upstroke, F_{int}, was measured as 12.44 N [14]; since the ornithopter has two wings then the integrated force acting on one wing is 6.22 N. The static load applied to the tip compliant hinge, F, was then assumed to be equal to the integrated force acting on the whole wing, namely 6.22 N [10].

A multi-objective genetic algorithm (NSGA-II) was implemented to solve the optimization problem. The shape of the compliant hinge was defined by control points, shown as black dots in figure 6(a). Nineteen control points were used to represent the inner and outer curves of the compliant hinge, with each of the control points spaced 10° apart. There were 38 decision variables, 19 inner radii, R_{in} (figure 6(a)), and 19 outer radii, R_{out} (figure 6(a)), which represent the radial coordinates of the control points. One of the solutions of the genetic algorithm is shown (as black lines) in figure 6(b). The shape of this optimal compliant hinge is shown compared to a semi-circular hinge for reference (shown as dotted blue lines). The optimization result is useful in that it tells us that the optimal hinge shape is nearly semi-circular, as opposed to some other shape such as elliptical or tapered. At the proposed scale, the performance of the semi-circular hinge and the optimized hinge are nearly the same. Such semi-circular hinges were used in the design of the first generation compliant spine prototype.

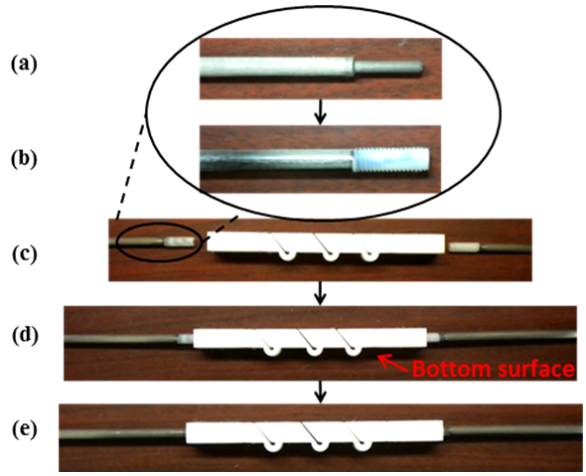

Figure 7. The compliant spine was attached to the spar (a) with 10–32 nylon bolts. The bolts were glued to both ends of the spar as shown in (b) and (c). Then the spars were screwed into the ends of the spine as shown in (d) and (e).

After determining the shape of a single compliant joint, an finite element analysis was used to determine the exact hinge dimensions and the number of compliant joints required to achieve the desired spine tip bending deflection of 8.42 mm, as explained above [15]. The analysis showed that three hinges were sufficient to realize the aforementioned bending deflection without exceeding the stress constraint, and thus the compliant spine prototype described in section 3 contained three compliant joints (figure 7).

3. Experimental evaluation

Based on the preliminary quasi-static analyses and optimization, an acceptable compliant spine design was selected for

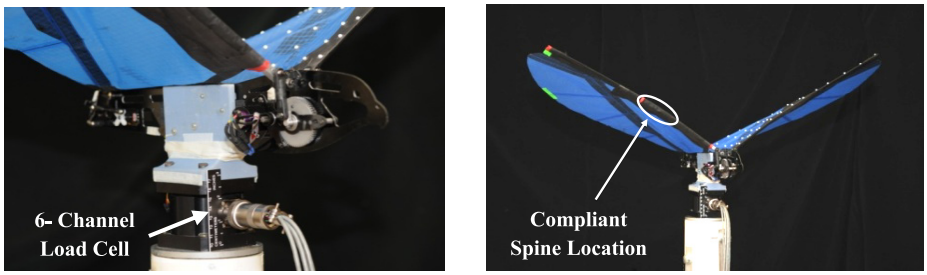

Figure 8. (a) Test ornithopter mounted on a six channel load cell to measure the lift and thrust produced at various flapping frequencies. (b) The compliant spine was inserted at the leading edge spar of the test ornithopter at 37% of the wing half span to mimic the function of an avian wrist.

prototyping and testing. The compliant spine consisted of three compliant hinges, with each compliant hinge consisting of two concentric semi-circles. The radius of the inner semi-circle was 1 mm and the radius of the outer semi-circle was 4 mm. Thus each hinge had a uniform thickness of 3 mm. The contact gap (g_c) was 0.762 mm (0.03″), the smallest gap that could be achieved using the water jet machining process, and the contact angle (φ) was 130°. This compliant spine was made of Delrin and was attached to the spar using 10–32 nylon bolts as shown in figure 7. The surface of the compliant spine with the compliant hinges is the bottom surface (figure 7(d)). In the ornithopter, this bottom surface is aligned with the wing lower surface using the joint at the wing root. This joint connects the spar and the flapping mechanism. The test ornithopter is a commercially available Park Hawk Model, which has a wing span of 1.07 m (42″). The ornithopter's mass without any payload is 425 g. It has a flapping rate between 4 and 6 Hz, a forward speed range of 10–30 km h^{-1}, and a distance range of 0.8 km [14]. The performance of the test ornithopter was measured with and without the compliant spine inserted into the leading edge spars. Three performance metrics were selected as a basis of comparison for the test ornithopter: (1) the required electric power, (2) the lift and thrust produced during one flapping cycle, and (3) the wingtip and spine tip deflections during the up and down strokes. This section describes the experimental setup and results related to these three performance metrics.

3.1. Experimental setup

The first performance metric is the electric power used by the flapping mechanism. In order to calculate the electric power, both the current and the voltage drawn from the power supply during flapping were measured. An in-house built constant voltage power supply was used for all of the experiments; hence the supply voltage was fixed at 12.27 V. In order to measure the current, a CQ-121E current sensor manufactured by Asahi Kasei Cooperation was used. The sensor was mounted in series between the power supply and the electric speed controller. Once the current and the voltage were measured, the electric power consumed by the ornithopter at various flapping frequencies was calculated.

The second set of performance metrics are the lift and thrust produced by the ornithopter. A six degree of freedom strain gauge transducer manufactured by Advanced Mechanical Technology Inc. was used to measure the lift and thrust produced by the test ornithopter at various flapping frequencies, with and without the compliant spine inserted in the leading edge spars. Figures 8(a) and (b) show the test ornithopter mounted on the load cell.

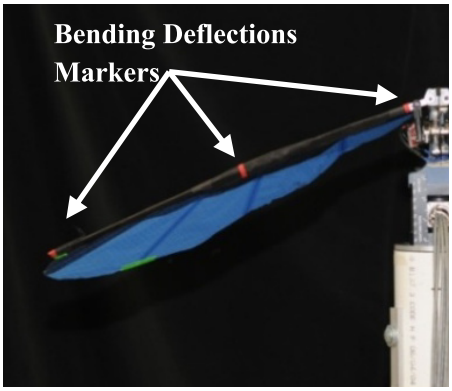

Figure 9. Red markers at the wing leading edge used for capturing wing bending deflections at the wing root, the compliant spine tip and the wing tip.

The third set of performance metrics are the wing tip and spine tip bending deflections. To capture the bending deflections of the wing during the up and down strokes, three red markers were placed on the leading edge spar. One marker was placed at the wing root, another was placed at the location of the compliant spine tip and a third marker was placed at the wing tip, as shown in figure 9. The camera time stamp was used to determine the frames that included the mid downstroke and upstroke kinematics, in the future a stroke angle sensor will be used to achieve a more accurate estimation of the wing position.

3.2. Experimental results

Data was collected at various flapping frequencies, where the flapping frequency was controlled by the throttle position on a remote control radio transmitter. Figures 10(a) and (b) show the electric power consumed by the ornithopter at various flapping frequencies, and the flapping frequency versus the percentage throttle, respectively. The 'solid' data corresponds to the performance of the ornithopter with the solid leading edge spar without the compliant spine insert, and the 'compliant' data corresponds to the performance of

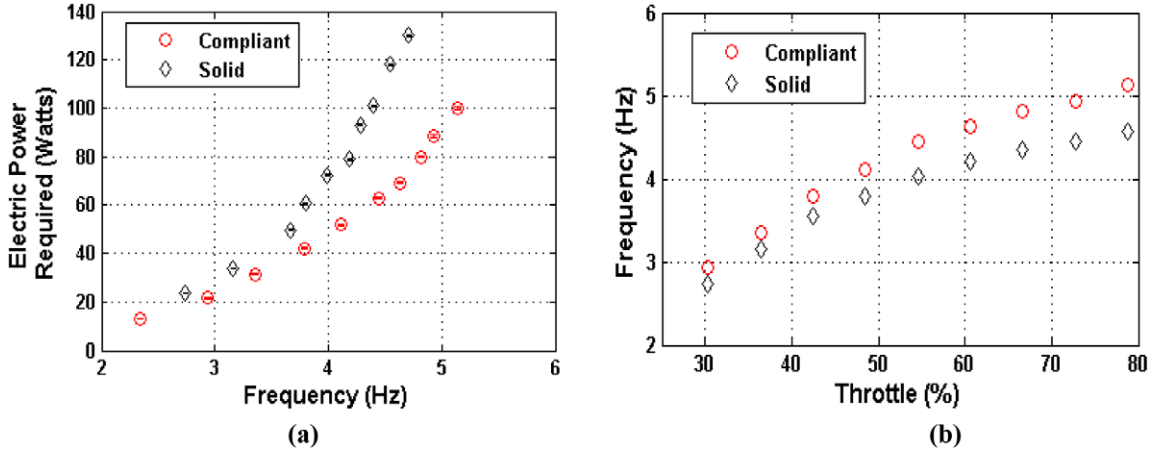

Figure 10. (a) The electric power required versus flapping frequency plot shows that the ornithopter with the compliant spine inserted in its wings ('compliant') uses less electric power than the ornithopter with the solid spar for any given flapping frequency. (b) The ornithopter with the compliant spine inserted in its wing ('compliant') flaps at a higher frequency than the ornithopter with the solid spar. The increase in flapping frequency can lead to thrust gains.

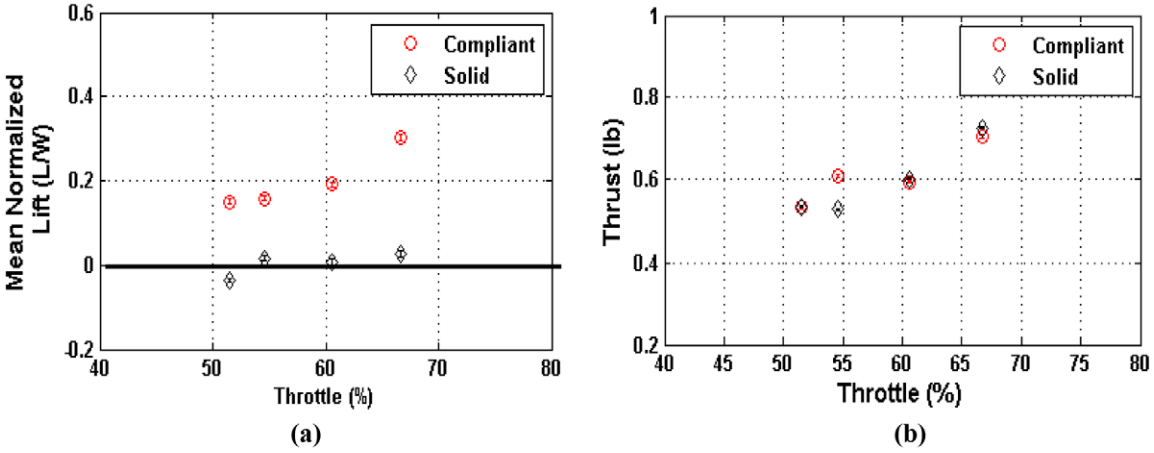

Figure 11. (a) The ornithopter with the compliant spine inserted in its wings produces more net mean lift than the ornithopter without the compliant spine for any given throttle setting. (b) The thrust versus throttle position plot shows that there are no thrust penalties due to the insertion of the compliant spine.

the ornithopter with the compliant spine inserted in the wings leading edge spar.

From figure 10(a), it can be observed that the test ornithopter with the compliant spine insert consumes less power than it does without the compliant spine, for all flapping frequencies. The focus of this work is centered on steady level flight. The steady level flight flapping frequency of the test ornithopter has been previously determined using minimum power and drag curves to be approximately 4.7 Hz in [14]. At 4.7 Hz the power savings due to the presence of the compliant spine is 44.7%. Also figure 10(b) shows that the ornithopter with the compliant spine inserted in its wings flapped at a higher flapping frequency for all throttle inputs. The fact that the ornithopter flapped at a higher frequency for a given throttle input is also attributed to this power expenditure reduction. Therefore flapping at a higher frequency may also produce concomitant thrust improvements.

Second, the lift and thrust were measured at various flapping frequencies for one wing beat cycle. The mean lift and thrust over one flapping cycle was calculated and the mean lift was normalized by the test ornithopter's weight. In previous work, it was determined that the mean induced lift produced by the test ornithopter when it is clamped to the load cell at zero forward speed and zero angle of attack is in fact zero [14]. This is due to the symmetry between the up and down strokes; the ornithopter produces an equal amount of positive and negative lift during the down and up strokes, making the mean lift zero. The results shown in figure 11(a) for the solid spar confirm these previous results. The same figure also shows that by inserting the compliant spine into the spars, an asymmetry is introduced between the up and down strokes which causes an increase in the mean lift. Moreover at the steady level flight flapping frequency of 4.7 Hz, the ornithopter with the compliant spine produced mean lift supporting 16% of its body weight. This lift gain could not be produced under the same conditions with a solid leading edge wing spar. This increase in mean lift can be directly translated into improved payload capability.

Although lift gains due to extreme wing bending deflections during the upstroke have been reported in previous passive wing morphing experiments [8], they were accompanied by severe thrust penalties. A goal of the current

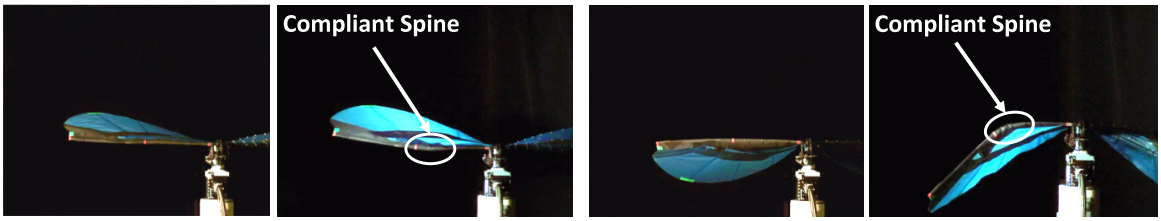

Figure 12. (a) Wing bending deflections at mid downstroke for the ornithopter with the solid spar, i.e., without the compliant spine. (b) Wing bending deflections at mid downstroke for the ornithopter with the compliant spine. Both (a) and (b) show comparable deformation indicating that the compliant spine is acting like the solid spar. (c) Wing bending deflections at mid upstroke for the ornithopter with the solid spar, i.e., without the compliant spine. (d) Wing bending deflections at mid upstroke for the ornithopter with the compliant spine. The ornithopter with the compliant spine exhibits large bending deflections when compared with the ornithopter with the solid spar.

Table 1. Bending deflections at the location of the compliant spine tip relative to the wing root. (Note: negative bending is upwards bending, positive bending is downwards bending.)

Wing position	With compliant spine (cm)	Without compliant spine (cm)	Difference in deflections (cm)
Mid downstroke	−3.41	−2.57	−0.84
Mid upstroke	4.07	0.72	3.36

work is to maintain the lift gains while mitigating the thrust penalties. Thus the effect of the presence of the compliant spine on the mean thrust produced by the test ornithopter was evaluated. Figure 11(b) shows that for any given throttle input, the mean thrust produced by the ornithopter with and without the compliant spine are similar, hence it is concluded that the compliant spine was successful at producing lift gains without incurring any significant thrust penalties.

Lastly the wing kinematics of the solid and compliant spars captured using high speed photography are compared. The compliant spine is designed to bend during the upstroke while remaining stiff (i.e., mimicking a solid spar) during the downstroke. Figure 12 compares the bending deflections of the wing with the compliant and solid spars at mid downstroke and mid upstroke. From figure 12(b) it can be seen that during the downstroke there is minimal deflection due to the contact surfaces in the compliant joints, while figure 12(d) shows that during the upstroke, the compliant spine bends as desired. This large bending deflection during the upstroke minimizes the drag penalties.

Both figures 12(a) and (b) show comparable deformation during the downstroke indicating that the compliant spine is acting like the solid spar, while figures 12(c) and (d) show that the wing with the compliant spine deflects more than that without the compliant spine during the upstroke. Table 1 shows the bending deflections at the location of the compliant spine tip relative to the wing root for the wing with and without the compliant spine at a flapping frequency of 4.7 Hz. These deflections were calculated by determining the difference between the vertical location of the middle bending deflection marker and the root bending deflection marker, mentioned in section 3.1, for the wing with and without the compliant spine.

The data in table 1 along with figure 12 show that during the downstroke the bending deflection of the wings with and without the compliant spine are similar. Meanwhile during the upstroke, the bending deflection of the wing with the compliant spine is larger than the wing without the compliant spine. The bending deflections noticed during the upstroke due to the presence of the compliant spine lead to a reduction of the wing relative surface area and therefore a decrease in the amount of negative lift and drag produced during that portion of the wing beat cycle. Moreover, during this experiment some twist was noticed as a result of the presence of the compliant spine. The induced twist cannot be quantified using the current experimental setup but will be investigated more carefully in the future.

4. Conclusions and future work

The overall goal of this work was to improve the steady level flight performance of ornithopters via passive wing morphing using a novel compliant spine. A quasi-static optimization was carried out and one of the designs resulting from this optimization was tested as a proof of concept. The presence of the compliant spine in the ornithopter wing was found to introduce an asymmetry between the upstroke and the downstroke. For any given flapping frequency, the ornithopter with the compliant spine consumed less electric power than the same ornithopter without the compliant spine. It was also found that for any given throttle input, the ornithopter with the compliant spine flapped at a higher flapping frequency, produced more mean lift and did not incur any thrust penalties when compared to the ornithopter without the compliant spine. Moreover, at the flapping frequency of interest, 4.7 Hz, the ornithopter with the compliant spine achieved 44.7% reduction in the power required and 16% lift gain. Also testing the ornithopter with the compliant spine inserted in its wings demonstrated that the bending deflection presented an asymmetry between the up and down strokes, resulting

in overall performance improvements. Thus the steady level flight performance was improved due to the presence of the compliant spine.

However due to the nature of the application of flapping wing flight, dynamic effects have to be taken into consideration in order to accurately simulate and predict the behavior of the compliant spine. Therefore, ongoing work includes development of a multi-objective optimization procedure that incorporates dynamic effects in the design of the compliant spine [15]. Also both bench-top and in-flight testing of the compliant spine designs resulting from the dynamic optimization will be conducted. Flight testing is necessary because while the bench-top tests are limited by the ornithopter being clamped to a load cell with zero angle of attack and zero forward speed; in-flight testing will allow us to determine the full effect of the presence of the compliant spine and passive morphing on the ornithopter's performance.

Acknowledgments

The authors gratefully acknowledge the support of AFOSR grant number FA9550-09-1-0632. The computational work was supported in part through instrumentation funded by the National Science Foundation through grant OCI—0821527. The resources of the NASA Langley Research Center and photographer Paul Bagby at the center are appreciated. Also the authors are grateful for the support of the Pennsylvania State University, University of Maryland and the Morpheus Lab.

References

[1] Shyy W, Berg M and Ljungqvist D 1999 Flapping and flexible wings for biological and micro air vehicles *Prog. Aero. Sci.* **35** 455–505

[2] Tobalske B W and Dial K P 1996 Flight kinematics of black-billed magpies and pigeons over a wide range of speeds *J. Exp. Biol.* **199** 263–80

[3] Tobalske B W 2000 Biomechanics and physiology of gait selection in flying birds *Physiol. Biochem. Zool.* **73** 736–50

[4] Fenelon M A A and Furukawa T 2010 Design of an active flapping wing mechanism and a micro aerial vehicle using a rotary actuator *Mech. Machine Theory* **45** 137–46

[5] McDonald M and Agrawal S K 2010 Design of a bio-inspired spherical four-bar mechanism for flapping-wing micro air-vehicle applications *J. Mech. Robot.* **2** 6

[6] Cox A, Monopoli D, Goldfarb M and Garcia E 1999 *Development of Piezoelectrically Actuated Micro-Aerial Vehicles* (Boston, MA: Society of Photo-Optical Instrumentation Engineers) pp 101–8

[7] Mueller D, Gerdes J W and Gupta S K 2009 Incorporation of passive wing folding in flapping wing miniature air vehicles *Int. Design Engineering Technical Conf. Computers and Information in Engineering Conf. (San Diego, CA)*

[8] Billingsley D, Grauer J and Hubbard J 2009 *Testing of a Passively Morphing Ornithopter Wing (AIAA AUU Seattle, Washington)*

[9] Brown R H J 1952 *The Flight of Birds: Wing Function in Relation to Flight Speed* Zoological Department, University of Cambridge

[10] Tummala Y, Wissa A, Frecker M and Hubbard J E Jr. 2010 Design of a passively morphing ornithopter wing using a novel compliant spine *Proc. Smart Materials, Adaptive Structures and Intelligent Systems Conf. (Philadelphia, PA)*

[11] Dupont, 2011 http://plastics.dupont.com/plastics/pdflit/americas/delrin/230323c.pdf

[12] Olympio K R 2006 Design of a passive flexible skin for morphing aircraft structures *MS Thesis* The Pennsylvania State University

[13] Wissa A, Tummala Y, Hubbard J E Jr and Frecker M 2011 Testing of novel compliant spines for passive wing morphing *Proc. Smart Materials, Adaptive Structures and Intelligent Systems Conf. (Scottsdale, AZ)*

[14] Harmon R 2009 Aerodynamic modeling of flapping membrane wing using motion tracking experiments, aerospace engineering *Master's Thesis* College Park, University of Maryland

[15] Tummala Y, Wissa A, Frecker M and Hubbard J E Jr 2011 Design optimization of a compliant spine for dynamic applications *Proc. Smart Materials, Adaptive Structures and Intelligent Systems Conf. (Scottsdale, AZ)*